Fast "*Operando*" Electron Nano-Tomography

Lucian Roiban[1], Shiwen Li[2], Mimoun Aouine[2], Alain Tuel[2], David Farrusseng[2],

Thierry Epicier[1,2]*

[1]Univ Lyon, INSA-Lyon, Université Claude Bernard Lyon I, UMR5510 CNRS, MATEIS, Bât. Blaise Pascal, 7, Avenue Jean Capelle, 69621 Villeurbanne cedex France

[2] Univ Lyon, Université Claude Bernard Lyon I, Ircelyon, UMR5256 CNRS, 2, Avenue Albert Einstein, 69100 Villeurbanne France

*thierry.epicier@insa-lyon.fr

ABSTRACT

Electron Tomography in Transmission Electron Microscopy provides valuable tri-dimensional structural, morphological and chemical information of condensed matter at nanoscale. Current image acquisitions require at least tens of minutes, which prohibits the analysis of nano-objects evolving rapidly such as under dynamic environmental conditions. Reducing the acquisition duration to tens of seconds or less permits to follow in 3D the same object during its evolution under varying temperatures and pressures. We report *Operando* Electron Nano-Tomography using image series acquired in less than 230 seconds instead of typically 15 minutes in the best cases so far. The *in-situ* calcination of silica zeolites encaging silver nanoparticles, a catalytic nano-system of potential interest for, e.g., nuclear waste treatments or selective heterogeneous catalysis, was successfully studied. Kinetic environmental *Operando* tridimensional Electron Microscopy becomes possible, as well as real time observation of beam sensitive samples (polymers, biological objects) without prior preparation which reduces their contrast and reactivity.

Keywords: *Operando* electron nano-tomography, environmental transmission electron microscopy (ETEM), heterogeneous catalysis, Ag nanoparticles, in situ calcination, silicates.

SECOND ABSTRACT

The development of nanotechnologies leads to a constant need of better characterisation of shapes and morphologies of nano-objects, nano-materials, nano-particles at the appropriate scale, that is a sub-micrometer or nanometer level. These sizes impose Transmission Electron Microscopy technique, an unsurpassed technique to study condensed matter at such a spatial resolution. Since these systems are aimed to be used in 'real life', it is further of the greatest importance to perform this analysis in their natural environment, or as close as possible to the conditions under which they are intended to be used. As a typically relevant example here, catalytic systems are developed for making chemical reactions possible, or improving their efficiency, by really manipulating gas molecules, most generally at high temperatures and of course a given gas pressure. Ideally, these investigations should be conducted in 3D: flawed interpretation or measurements are current in 2D images where a tridmensional object is simply projected in a viewing direction which does not give access to the position of elementary features along, precisely, this viewing direction (this may be up to the point where the projection evokes a totally different object from the real one and this has been used for entertainment for many years - see the nice example of hand shadows by Henry Bursill in the XIXth century www.gutenberg.org/files/12962/12962-h/12962-h.htm -). 3D analyses can be performed in different ways, a current approach with microscopy techniques is the so-called 'tilted tomography', where 2D projections of the object are recorded under several orientations over a large angular amplitude, which allows the volume to be numerically rebuilt with the help of dedicated reconstruction softwares.

Summarizing this introduction leads to the goal of the present work: can we perform in situ 3D analyses of nano-catalysts under environmental conditions (temperature and gas pressure) in the transmission electron microscope (TEM)? A positive demonstration will be made using a specific nano-composite catalyst which will be literally burnt under oxygen inside an Environmental TEM. The ambitious goal of following in situ the morphological evolution of a nanometric object during an ongoing chemical reaction (or any other dynamic process) raises the question of the speed of image acquisition (during the sample rotation required in 'tilted tomography'). The duration of the whole acquisition must obviously be faster that the morphological changes of the sample in order to allow correct 3D reconstructions, and this is also what we focus on in the present contribution.

INTRODUCTION

The development of functional nanomaterials having different phases and structures with complex morphologies brought an increasing need for tri-dimensional (3D) characterization at the nanometric scale. In materials science, electron tomography (ET) has been consistently improved in the last decades and is now currently and routinely applied to the nanometric level (KOSTER et al., 2000; DE ROSIER and KLUG, 1968; FRANK, 2006; MÖBUS and INKSON, 2007; BARCENA and KOSTER, 2009; MIDGLEY and DUNIN-BORKOWSKI, 2009; EPICIER, 2014; ERSEN et al., 2015). Recent developments have further demonstrated the possibility of ET at the atomic resolution (VAN AERT et al., 2011; SCOTT et al., 2012; VAN DYCK et al., 2012), thus providing a complementary method to atom probe tomography (THOMPSON et al., 2007; LEFEBVRE et al., 2016).

ET consists in the acquisition of a series of projected images by tilting the sample over a large amplitude range, typically up to ±70°, or even more, using conventional high-tilt specimen holders, and ideally over a full ±90° range when cylindrical tip-like samples can be prepared (KAWASE et al., 2007). One of the main drawbacks of ET is the slow acquisition of the whole series of images. Depending on the imaging mode, a tilt series recording generally takes between 15 to 30 minutes in bright field mode (BF; ERSEN et al., 2008) and more than 2 hours in the Scanning or energy filtered modes (respectively STEM: MIDGLEY et al., 2006 and EFTEM: ROIBAN et al., 2012; ROIBAN et al., 2016).

Due to long exposure times during recording of projections, ET is thus not appropriate to the study of unprotected beam sensitive samples nor to *in situ* experiments. As a major example, environmental electron microscopy (ETEM) now permits *operando* observations of nanomaterials such as catalysts, the nanostructure of which usually evolves when environmental conditions change (pressure, temperature, oxidizing/reducing conditions). Obviously, if the nanostructure changes within the acquisition period, any 3D reconstruction becomes meaningless. For beam-sensitive or biological samples, the 3D study is nonetheless possible by using low-dose techniques (ROIBAN et al., 2016), protecting materials from contact with the environment (PRIETO et al., 2013) or using cryogenic conditions (SCHUR et al., 2015). However, protection does not allow observations at high temperatures, such as the reconstruction of catalytic surfaces under reaction conditions.

While fast projections recording is possible for X-ray tomography especially when performed in high flux synchrotron sources (BUFFIÈRE et al., 2014), ET remains up to now too slow to follow the dynamical morphological evolution of materials in intermediate states during a catalytic reaction. Besides problems related to the chemical stability of the samples, some technical difficulties simply result from the displacements of the sample during the tilting procedure and the acquisition time itself. However since recording media enabling to capture images at high frequencies (e.g. several Hertz) with a sufficient signal-to-noise ratio are already commercially available, it can be anticipated that real time or time resolved electron tomography will soon be possible in a TEM, at least in the bright field imaging mode when applicable (ZEWAIL and THOMAS, 2010).

In almost all cases, materials analyzed in TEM are under high vacuum, which is obviously not their natural environment when they are used under real working conditions. This is particularly true for solid catalysts which are essentially operating in special environmental conditions, with reactive gases such as hydrocarbons above atmospheric pressure and temperatures of hundreds of degree C. It is of the greatest importance to be able to follow the 3D nanostructure evolution of a catalyst in the course of its calcination or activation during oxidizing/reducing treatments or in environmental conditions which are representative of reaction conditions. Attempts have been recently tried to do it 'post-mortem', i.e. at different stages of an ex-situ treatment, such as the calcination of a porous silica zeolite (ARSLAN and STACH, 2012) or electrochemical ageing of Pt−Co Fuel Cell nano-catalysts (YU et al., 2012). Although very valuable, such approaches however do not allow to follow directly any modification, neither identify transient metastable

configurations, as it is possible in true *operando* analysis in a dedicated Environmental TEM (ETEM: JINSCHEK, 2014).
The ETEM associates a nano-reactor and a Transmission Electron Microscope (TEM), making possible the study of materials at nanoscale, and even at atomic resolution (TAKEDA et al., 2015) under gas atmosphere and temperature close to working conditions. To our best knowledge, ET has not been yet carried out in environmental conditions due to the long duration of tilt series acquisition which may trivially not be compatible with the possibly rapid kinetics of a chemical reaction at a nanoscale. Under environment conditions, 3D chemical information can be preserved only if the recording time of the tilt series is as short as possible. Another advantage of fast projections recording also will be to reduce any beam damage for sensitive or biological samples.

In this work, we show pioneer attempts to perform rapid ET of nano catalysts under environmental gas and temperature conditions at 300 kV in an ETEM. For demonstration purpose, we have selected a beam sensitive material, which obviously has to be studied "as is" in order to conserve its catalytic activity. Without any special preparation, a single object consisting in a group of five mesoporous silica hollow zeolite encaging Ag nanoparticles (NPs) has been followed by *Operando* Electron Nano Tomography (OENT) in high vacuum at 20°C and under controlled environmental conditions (oxygen flow) at 280°C and 450°C.

EXPERIMENTAL BACKGROUND

Synthesis of hollow zeolites encapsulated Ag nanoparticles

The 'test' nano-catalyst used to demonstrate the feasibility of OENT consists in hollow silicalite-1 crystals encapsulated Ag nanoparticles (Ag@ silicalite-1). Metal nanoparticles encapsulated in hollow mesoporous zeolite crystals represent a very interesting class of nano-membrane reactors in which the reaction is essentially governed by the permeability of the shell (FARRUSSENG and TUEL, 2016). These nano-catalysts are the subject of continuous development for applications such as nuclear waste treatments or selective heterogeneous catalysis (DELIERE et al., 2016; www.molecularproducts.com/us/ionex.htm). Indeed, particles are only accessible to molecules that can diffuse through the zeolite walls, i.e. with a kinetic diameter smaller than the pore size.

Ag@ silicalite-1 were synthesized following a dissolution/recrystallization method reported in a previous publication (LI et al., 2013). Briefly, silicalite-1 nanocrystals (150-200 nm in size) were impregnated with a solution of silver nitrate $AgNO_3$ using a wetness impregnation method (1 wt. % Ag). After drying at 100°C overnight, crystals were dispersed in a solution of tetrapropylammonium hydroxide TPAOH (10 mL of 0.5M solution/g zeolite) and heated at 170°C under static conditions for 24 hours. The central part of the crystals is selectively dissolved, leading to hollow silica structures in which Ag^+ cations become reduced and crystallize as entrapped metal nanoparticles.

As a consequence, internal particles are totally isolated from outside and accessible only to molecules that can diffuse through the zeolite pores, i.e. with a kinetic diameter smaller than 0.6 nm in the particular case of MFI zeolites. However, the partial recrystallization of the zeolite walls during the treatment with TPAOH makes that the solid needs to be calcined at high temperature to liberate the porosity from occluded organic molecules. After encapsulation, the partial recrystallization of the zeolite makes that pores are blocked by organic molecules and the latter have to be removed by calcination at high temperature to release the porosity. Since particles are generally much larger than zeolite pores, they cannot, in principle, escape from the cavity. They are subsequently protected against extensive sintering outside the silicalite. However, in contrast to many other noble metals such as Au, Pt, Pd, ex-situ treatments show that Ag particles

simultaneously are expelled out of the cavities and conversely re-appear out of the cavities when solids were calcined in air at temperatures typically above 500°C (LI, 2015). To better understand the phenomenon, it was thus particularly important to develop an *in situ* technique capable of studying the morphology and the location of these nanoparticles at the nanometer scale with temperature under oxygen pressure.

Microscopy work

Samples for TEM work were diluted in alcohol, the solution was placed in an ultrasonic bath for 5 minutes and a droplet was laid on a holey carbon microscopy grid.

Conventional, High Resolution, Scanning TEM observations and the environmental electron tomography analyses in *operando* mode were performed on a FEI TITAN environmental microscope (ETEM 80-300 keV,FEI, Hillsboro, OR, USA) equipped with a spherical aberration corrector of the objective lens.

The first fast tomography acquisition was performed at room temperature under a high vacuum of about 10^{-7} mbar using a dedicated ±80° single tilt tomographic Fischione (Export, PA, USA) sample holder. Considering the fact that silicalite-1 based materials are relatively sensitive to the electron beam and easily degrade under standard electron beam exposure conditions, preliminary irradiation experiments were performed in order to define reasonable imaging and acquisition conditions preserving the integrity of the samples. The video (SI_OENT_L-Roiban_et-al_speedX200.avi) illustrates the irradiation behaviour of a group of silica hollow zeolites submitted to a 4 minutes exposure at different electron fluxes: $1.1 \cdot 10^{7}$ $e^{-}nm^{-2}s^{-1}$, $4.4 \cdot 10^{6}$ $e^{-}nm^{-2}s^{-1}$ and $3.3 \cdot 10^{6}$ $e^{-}nm^{-2}s^{-1}$ respectively. Contrarily to the two first conditions, the last condition did not reveal any significant morphological evolution of the hollow silicates during the exposure to the electron beam; the corresponding electron flux and exposure time were then chosen as maximal limits to perform safe electron tomography analysis.

According to this preliminary experiment, the recording of a tilt series over an amplitude of 116° in less than 4 minutes was performed. The rotation speed of the goniometer was about 0.5°/s and the camera speed was set to 7 frames per second - fps - (UltraScan 2K US1000XP-P from Gatan, Pleasanton, CA, USA) meaning 0.15 s/image. Video sequences were recorded by grabbing the 8 bits display of the camera using the free software Camstudio v.2.0 (http://camstudio.org/) at a speed about 3 times faster than the camera refresh rate. The rotation of the goniometer was performed using a microscope function permitted in the advanced user mode; during the tilting sequence, image shift and focus correction was performed manually. After the acquisition of projections, a home-made software allowed duplicated frames to be eliminated, as well as the most blurred images.

OENT analyses were performed using a heating holder Gatan model 628 IN with an inconel furnace compatible with an oxidizing atmosphere. The same object has been heated up to a calcination temperature of 450°C under 1.8 mbar O_2.

Data analysis, volume segmentation and quantification

All tilted series acquired previously were post-aligned with the Imod software (KREMER et al., 1996) and the volume reconstructions were performed using 20 iterations of the OSAT algorithm implemented in Tomoj software (MESSAOUDI et al., 2007). Volume analyses and three

dimensional quantifications were performed using different tools available in ImageJ (http://imagej.nih.gov/ij/) and 3D Slicer software (FEDOROV et al., 2012).

TEM and ETEM RESULTS

Nanostructure of Ag@silicalite-1

TEM pictures from Figure 1 clearly show that the pores network of zeolites is ideally periodic (zeolites are thus considered as crystalline objects), and each box is actually a single crystal, in most cases without any visible crack or hole (Figure 1a-b)). The structure of the silicalite (orthorhomb**ic** unit cell, space group Pnma with a = 2.009, b = 1.9738, c = 1.3142 nm www.iza-structure.org/databases/) is more easily resolved in the STEM imaging mode which appeared to be less aggressive than the TEM mode regarding irradiation damage (Figure 1c-d)). As quoted in the Experimental Background section, Ag nanoparticles are expelled out of the silicialite cages after calcination in air (Figure 1e-f)); a significant increase in their size further occurs as a consequence of heating.

Fast tilt series acquisition

Continuous rotation tomography consists in recording the sample projections as a video sequence during the rotation of the goniometer. This approach constitutes a breakthrough with respect to the step-by-step tilting process which is the current and well-established procedure of ET. It is very easy to implement and the most efficient way to acquire a fast image tilt series. All parameters controlling this experimental setup were determined according to the following main constraints:

(i) The sample must not suffer detectable irradiation damages during the entire data collection time.

(ii) The signal-to-noise ratio (SNR) of all acquired frames has to be sufficient for the ET analysis.

(iii) The frame rate of the dynamic video sequence must be such that no significant blur degrades the quality of images.

(iv) The magnification and size of images have to be adapted to the spatial and numerical resolution needed for the material of interest.

A trial-and-error approach also allowed us to determine a suitable combination of all experimental parameters fulfilling previous constraints (i) to (iv). Regarding point (i): the degradation test carried out at room temperature under usual high vacuum allowed us to estimate that hollow crystals could support a 4 minutes beam exposure with a reasonable flux of $3.3.10^6$ $e^-/nm^2.s$ (see Supporting Information, section SI1). Under those conditions, an acquisition time of 0.2 s per frame leads to an acceptable SNR, thus respecting constraint (ii). A first fast tilting experiment illustrated by Figure 2 was recorded over a tilt range close to 120° in less than 4 minutes in vacuum at room temperature according to the conditions summarized in Table 1. After skipping duplicated and too much blurred images (point (iii); see Figure SI-1 in Supporting Information), 328 images were retained for the volume reconstruction representing 62% of the total images number and a mean angular resolution of 0.35°, a value much smaller than the typical 1° or 2° increment used in conventional tilting of electron tomography.

The last point (iv) concerns the resolution; the microscope magnification was adapted to obtain a pixel size of 0.8 nm. It was found that the resolution along the Z-axis remains close to 1.5 nm due to the well-known elongation effect caused by the missing wedge; this value remains typical for tilted ET. Figure 2b-c) show a core section extracted from the XY plane and the reconstructed model in which the hollow zeolite and Ag nanoparticles are represented in green and red, respectively. The Ag nanoparticle size distribution, estimated from a total of 56 particles, has an average of 6.1 nm (Figure 2d)). The diameter was estimated considering Ag nanoparticles as spheres and it appeared that only 2 particles among 56 (3%) were located outside, on the external surface of hollow zeolite crystals (Figure 2c)). Basal planes do not appear in the reconstructed model of silica cages due to the fact that their thickness is at the limit of the resolution along Z-axis of ET. Additional morphological features can be measured from this 3D analysis, e.g. the wall thickness of the silica cages, with an average diameter of ca. 150 nm, is varying between 4 and 34 nm (see Figure SI1 in the Supplementary Information file). This information is a valuable quantitative output from the tomography analysis. It is worth re-emphasizing that this study could not be performed successfully with a conventional step-by-step tilting procedure owing to the irradiation damage that the zeolites would have then suffered. This shows that fast tomography presents great advantages for beam sensitive samples and could thus be very beneficial for soft materials such as polymers or biological tissues. Moreover, it is a step closer to time resolved 3D analysis and especially under environmental conditions as developed in the next sub-section.

"*Operando*" Electron Nano-Tomography

The fast tomography approach has been extended to the study of the in situ calcination of hollow silicalite-1 cages containing Ag nanoparticles. To follow the evolution of both the silica bodies and the Ag NPs, three short time continuous tilt series were acquired from the same group of objects at 20°C, 280°C and 450°C as shown by Figure 3. Experimental conditions similar to those reported in Table 1 are summarized in Table 2. Due to the strong shadowing by the furnace edges at high tilt, the tilting amplitude was restricted to 67° between about -25° and 42°. All tilt series were acquired in around 2 minutes, precisely here 121, 106 and 116 seconds at 20°C, 280°C and 450°C respectively. At 20°C the tilt series was recorded in high vacuum. The cages exhibit main morphological and nanostructural characteristics as observed before: Ag NPs have an average size of 6.7 nm and only 3 particles (5% in number) are lying outside the hollow silica zeolites, mainly on their external surface (Figure 3a)). At 280°C under 1.8 mbar of O_2, some changes occur: most of the nanoparticles are still inside hollow zeolite crystals but their total number decreases from 56 to 41, whereas their average diameter increases up to 7.6 nm.

Interestingly, the 3D analysis permits to measure quite accurately that the total silver volume remains roughly constant around 14,600 nm^3 (14,592 nm^3 at 20°C and 14,772 nm^3 at 280°C). This finding confirms that nanoparticle growth occurred without loss of silver, in the limit of measurement accuracy (Figure 3b)), and this evolution proceeds mainly by the classical Ostwald ripening mechanism further identified in 2D at slightly higher temperatures (not reported here). Reaching the temperature of 450°C in O_2 produces a drastic change in the distribution of Ag NPs: their number considerably decreases to 15, with 12 of them (80% in number) outside the silica cages (Figure 3c)). This phenomenon can consistently be explained by the effect of oxygen on the cages. During the initial formation of hollow crystals and Ag NPs simultaneously at high temperature, part of the zeolite recrystallizes in the presence of TPA^+ cations. Such organic cations completely obstruct the pores of silicalite-1 and it is necessary to heat the zeolite in air at temperatures between 300 and 550°C to burn organics and liberate the porosity. When temperature reaches 450°C in the microscope, the oxygen flux leads to the combustion of organic molecules which were plugging the micropores of the zeolite. Then oxygen can reach the silver particles

which easily oxidize to form silver oxides. These oxides and particularly Ag_2O, known as the most stable AgO_x compound up to about 250°C, decompose and vaporize spontaneously at high temperature (L'VOV, 1999; ROY et al., 2007). This explains the rapid disappearance of Ag NPs from the cavities of the zeolite (well imaged in Figure 1a-c))[1]. It was simultaneously observed than new silver particles reform outside on the carbon supporting film, see Figure 4. These fresh silver NPs can reform there because of the efficient dissociation of O_2 molecules into atomic oxygen at their surface, which can further reacts with the carbon coating of the TEM grid, leading to the carbon gasification into volatile CO_2 (SEVERIN et al., 2009). This occurs at the interface between the Ag NPs and the carbon film, and the carbon consumption makes that silver NPs advance and create a trench on their path in the supporting film as it can be clearly seen on Figure 4. This is the so-called 'Pacman' effect previously observed in ETEM on a graphite support (BOOTH et al., 2011). During this process the silver particle remains crystalline but adopts a wavy front at the interface with the carbon support promoted by the intense atomic mobility at its surface owing to the gas-solid interaction (see section SI-4, Figure SI3).

SUMMARY AND CONCLUSIONS

Continuous rotation tomography and *Operando* Electron Nano-Tomography approaches have been successfully applied to the study of the calcination of Ag@ silicalite-1 nanocatalysts.

The evolution of this nanocomposite system has been followed in situ under oxygen up to 450°C in the ETEM. When the zeolite pores become totally free from organics during the calcination process, the oxygen flux produced in the microscope leads to a rapid oxidation of internal silver nanoparticles. Since any silver oxide is unstable typically above 250°C, it spontaneously decomposes and silver vapour is immediately expelled from the zeolite cavities. Consequently, metallic nanoparticles reform on the carbon film and carbon gasification induced by the dissociation of O_2 molecules at their surfaces leads to a progressive consumption of the carbon supporting film.

Clearly this complete scenario could only be accurately identified and understood through the present *operando* study. If classical and slow ET would have been carried out, the particle growth and relocation mechanisms could have been wrongly interpreted as the result of the zeolite degradation during images recording, which is obviously not the case according to the fast tomography results. Furthermore, the exact influence of the temperature during the activation process over the Ag nanoparticles and silicalites-1 would not have been determined.

The oxidation of the initial Ag NPs and their spontaneous ejection from the zeolite cages is undesirable as the zeolite walls are expected to control the accessibility to NPs by molecular sieving. The conclusion of the OENT study provides clear guidelines for the modification of synthesis protocol in order to prevent this shortcoming. The preparation protocol of Ag loaded hollow zeolite shall be modified so that the calcination treatment for removing the organic template shall be carried out before the encapsulation of Ag particles, such as by a post impregnation with a silver salt solution. It was not obvious to draw this conclusion without OENT analysis; indeed,

[1] this situation can be improved if the Ag loaded zeolite is heated in the presence of a reducing agent such as H_2 or under high vacuum: ex-situ experiments have shown that the catalysts are more stable under such conditions and that Ag NPs remain inside the cavities.

this behaviour in presence of oxygen is very specific for Ag among the series of noble and transition metals we have investigated: Ag, Au, Pt, Pd, Co, Ni, Fe (LI et al., 2013).

Clearly, OENT is a very promising approach and will allow breakthrough advances in *operando* studies of nano-catalysts system down to the nanometer scale. Although successful regarding the possibility to study the same object under different environmental conditions, the present OENT method suffers some limitations. The time resolution is here the main issue. In the present work, tilted image series with reasonable sharpness and signal-to-noise ratio have been acquired using a conventional camera for TEMs during a rotation sequence performed at a speed of about 0.5-0.6°/sec. The rotation speed is indeed strongly limited by the frame acquisition time permitted by the camera, about 0.2 s/frame in our study. Using the latest technical improvements of commercially available cameras much faster tilt series acquisitions are now possible; highly contrasted images can now be acquired at high frame rates with image acquisition times of a few ms with CMOS-based of direct electron detection cameras of the latest generation (OZDOL et al., 2015; MIGUNOV et al., 2015; NANNENGA, GONEN, 2016). Also, MEMS-based modern heating holders provide today a much better tilt capability up to at least ±70° without any shadowing of the sample (e.g. DENSsolutions, 2016). Our preliminary experiments using such recent equipments demonstrate that tomography tilt series can be possibly acquired in less that at least 5 seconds over a total tilting amplitude of 143 degrees under gas at high temperature in ETEM. A time limitation will finally be imposed by the mechanical stability of the microscope goniometer over the whole tilting range, a parameter difficult to control and improve at the present time.

Current work in progress on other catalytic systems show that OENT is readily applicable to kinetic studies of catalytic interactions in an environmental microscope. The potential interest of fast tomography is also anticipated for the 3D analysis of biological samples, especially to follow their evolution in conditions simulating their natural environment.

ACKNOWLEDGMENTS

Thanks are due to the CLYM (www.clym.fr) for its guidance in the ETEM project which was financially supported by the CNRS, the Région Rhône-Alpes, the 'GrandLyon' and the French Ministry of Research and Higher Education. The authors further acknowledge F.J. Cadete Santos Aires (IRCELYON, University Lyon I), C. Langlois (MATEIS, INSA-Lyon) and N. Blanchard (ILM, University Lyon I) for their help and fruitful discussions on the ETEM, and L. Burel (IRCELYON, University Lyon I) for her assistance in preparing samples. L.R. and T.E. acknowledge the support of the INSA-Lyon BQR project SPEE3D 2015-0020, the French Labex 'IMUST' (supported project in 2014) and the French ANR project n°15-CE09-0009-0 '3DCLEAN'.

REFERENCES

ARSLAN, I., STACH, E.A. (2012) Seeing atoms in three dimensions, Nature Materials 11, 911-912.

BARCENA, M., KOSTER, A.J. (2009) Electron tomography in life science, Seminars in Cell & Developmental Biology. 20, 920-930.

BOOTH, T.J., PIZZOCCHERO, F., ANDERSEN, H., HANSEN, T.W., WAGNER, J.B., JINSCHEK, J.R., DUNIN-BORKOWSKI, R.E., HANSEN, O., BØGGILD, P. (2011) Discrete dynamics of nanoparticle channelling in suspended graphene, Nano Lett. 11, 2689-2692.

BUFFIERE, J.Y., MAIRE, E., LUDWIG, W., SALVO, L., BOLLER, E., GOUILLART, E., ROUX, S. (2014) Tomographie utilisant le rayonnement synchrotron. In Imagerie 3D en Mécanique des Matériaux MIM Hermès Science,163-191.

DE ROSIER, D. J., KLUG, A. (1968) Reconstruction of three dimensional structures from electron micrographs. Nature 217, 130-134.

DELIERE, L., COASNE, B., TOPIN, S., GRÉAU, C., MOULIN, C., FARRUSSENG, D. (2016) Breakthrough in xenon capture and purification using adsorbent-supported silver nanoparticles, Chem. Eur. J. 22, 9660-9666.

DENSsolutions, (2016) EMheaterchips, http://denssolutions.com/products/heating/wildfire-s5-for-fei-microscope/ (URL).

EPICIER, T. (2014) Tomographie Électronique in Imagerie 3D en Mécanique des Matériaux. MIM Hermès Science, 83-124.

ERSEN, O., FLOREA, I., HIRLIMANN, C., PHAM-HUU, C. (2015) Exploring nanomaterials with 3D electron microscopy. Materials Today, 18, 7, 395-408.

ERSEN, O., PARMENTIER, J., SOLOVYOV, L. A., DRILLON, M., PHAM-HUU, C., WERCKMANN, J., SCHULTZ, P. (2008) Direct Observation of Stacking Faults and Pore Connections in Ordered Cage-Type Mesoporous Silica FDU-12 by Electron Tomography. J. Am. Chem. Soc. 130, 49, 16800-16806.

FARRUSSENG, D., TUEL, A. (2016) Perspectives on zeolite-encapsulated metal nanoparticles and their applications in catalysis, New J. Chem. 40, 3933- 3949.

FEDOROV, A., BEICHEL, R., KALPATHY-CRAMER, J., FINET, J., FILLION-ROBIN, J-C., PUJOL, S., BAUER, C., JENNINGS, D., FENNESSY, F., SONKA, M., BUATTI, J., AYLWARD, S.R., MILLER, J.V., PIEPER, S., KIKINIS, R. (2012) 3D Slicer as an image computing platform for the quantitative imaging network, Magn Reson Imaging. 30 (9), 1323-41; www.slicer.org/ (URL).

FRANK, J. (2006) Electron Tomography: Methods for Three-Dimensional Visualization of Structures in the Cell. Springer: New York, ed. 2.

JINSCHEK, J. (2014) Advances in the environmental transmission electron microscope (ETEM) for nanoscale in situ studies of gas–solid interactions. Chem Commun. 50, 2696-2706.

http://camstudio.org/ (URL).

http://imagej.nih.gov/ij/ (URL).

KREMER, J.R., MASTRONARDE, D.N., MC INTOSH, J.R. (1996) Computer visualization of three-dimensional image data using IMOD. J Struct Biol 116, 71-76.

KAWASE, N., KATO, M., NISHIOKA, H., JINNAI, H. (2007) Transmission electron microtomography without the "missing wedge" for quantitative structural analysis. Ultramicroscopy 107, 1, 8-15.

KOSTER, A. J., ZIESE, U., VERKLEIJ, A. J., JANSSEN, A. H., DE JONG, K. P. (2000) Three dimensional Transmission Electron Microscopy a novel imaging and characterization technique with nanometer scale resolution for materials Science. J. Phys. Chem. B 104, 9368-9370.

L'VOV, B. V. (1999) Kinetics and mechanism of thermal decomposition of silver oxide, Thermochimica Acta 333, 13-19.

LEFEBVRE, W., VURPILLOT, F., SAUVAGE, X. (2016) Atom Probe Tomography, Put Theory into Practice, Academic Press: New York, ed. 1.

LI, S., BUREL, L., AQUINO, C., TUEL, A., MORFIN, F., ROUSSET, J.L., FARRUSSENG, D. (2013) Ultimate size control of encapsulated gold Nanoparticles. Chem. Commun., 49, 8507.

LI, S., (2015), Metal nanoparticles encapsulated in membrane-like zeolite single crystals: application to selective catalysis, PhD, Université Claude Bernard - Lyon I, <NNT: 2015LYO10057>. <tel-01163661>

MESSAOUDI, C., BOUDIER, T., SORZANO, C.O.S., MARCO, S. (2007) TomoJ: tomography software for three-dimensional reconstruction in transmission electron microscopy. CBMC Bioinformatics 8, 288.

MIDGLEY, P.A., WEYLAND, M., YATES, J.V., ARSLAN, I., DUNIN-BORKOWSKI, R.E., THOMAS, J.M. (2006) Nanoscale scanning transmission electron tomography. J. of Microscopy 223, 185-190.

MIDGLEY, P.A., DUNIN-BORKOWSKI, R.E. (2009) Electron tomography and holography in materials science. Nature Materials, 8, 271-280.

MIGUNOV, V., RYLL, H., ZHUGE, X., SIMSON, M., STRÜDER, L., BATENBURG, K. J., HOUBEN, L., DUNIN-BORKOWSKI, R. (2015). Rapid low dose electron tomography using a direct electron detection camera, Scientific Reports, 5, 14516.

MÖBUS, G., INKSON, B.J. (2007) Nanoscale tomography in materials science, Materials Today. 10-12, 18-25.

NANNENGA, B.L., GONEN, T. (2016) MicroED opens a new era for biological structure determination, Current Opinion in Structural Biology, 2016, 40:128-135.

OZDOL, V.B., GAMMER, C., JIN, X.G., ERCIUS, P., OPHUS, C., CISTON, J., MINOR, A. M. (2015) Strain mapping at nanometer resolution using advanced nano-beam electron diffraction, Appl. Phys. Lett. 106, 253107.

PRIETO, G., ZEČEVIĆ, J., FRIEDRICH, H., DE JONG, K.P., DE JONGH, P. E. (2013) Towards stable catalysts by controlling collective properties of supported metal nanoparticles. Nature Materials 12, 34-39.

ROIBAN, L., SORBIER, L., PICHON, C., BAYLE-GUILLEMAUD, P., WERCKMANN, J., DRILLON, M., ERSEN, O. (2012) Three-dimensional chemistry of multiphase nanomaterials by Energy-Filtered Transmission Electron Microscopy Tomography. Microsc. Microanal. 18, 1118-1128.

ROIBAN, L., SORBIER, L., HIRLIMANN, C., ERSEN, O. (2016) 3D chemical distribution of titania–alumina catalyst supports prepared by the swing-ph method. ChemCatChem 8, 1651-1657.

ROIBAN, L., FORAY, G., RONG, Q., PERRET, A., IHIAWAKRIM, D., MASENELLI-VARLOT, K., MAIRE, E., YRIEIX, B. (2016) Advanced three dimensional characterization of silica-based ultraporous materials. RSC Adv. 6, 10625-10632.

ROY, R., HOOVER, M. R., BHALLA, A. S., SLAWECKI, T., DEY, S., CAO, W., LI, J., BHASKAR, S. (2007) Ultradilute Ag-aquasols with extraordinary bactericidal properties: role of the system Ag–O–H_2O, Mater. Res. Innov. 11, 3-18.

SCHUR, F.K.M., HAGEN, W. J. H., RUMLOVÁ, M., RUML, T., MÜLLER, B., KRÄUSSLICH, H.G., BRIGGS, J.A.G. (2015) Structure of the immature HIV-1 capsid in intact virus particles at 8.8 Å resolution. Nature 517, 505-508.

SCOTT, M.C., CHEN, C.C., MECKLENBURG, M., ZHU, C., XU, R., ERCIUS, P., DAHMEN, U., REGAN, B. C., MIAO, J. (2012) Electron tomography at 2.4-Angström resolution. Nature, 483, 444-447.

SEVERIN, N., KIRSTEIN, S., SOKOLOV, I. M., RABE, J. P. (2009) Rapid trench channeling of graphenes with catalytic silver nanoparticles. Nano lett. 9, 457-461.

TAKEDA, S., KUWAUCHI, Y., YOSHIDA, H. (2015) Environmental transmission electron microscopy for catalyst materials using a spherical aberration corrector. Ultramicroscopy 151, 178–190.

THOMPSON, K., FLAITZ, P. L., RONSHEIM, P., LARSON, D. J., KELLY, T. F. (2007) Imaging of arsenic cottrell atmospheres around silicon defects by three-dimensional atom probe tomography. Science 317, 1370.

VAN AERT, S., BATENBURG, K.J., ROSSELL, M.D., ERNI, R., VAN TENDELOO, G. (2011) Three-dimensional atomic imaging of crystalline nanoparticles. Nature 470, 374-377.

VAN DYCK, D., JINSCHEK, J.R., CHEN, F. R. (2012) 'Big Bang' tomography as a new route to atomic-resolution electron tomography. Nature, 486, 243-246.

www.iza-structure.org/databases/ (URL); IZA-SC Database of Zeolite Structures, CIF file of MFI model from Ch. Baerlocher, L.B. McCusker.

www.molecularproducts.com/us/ionex.html (URL): Nuclear air cleaning, Capture of radioiodines in radioactive gas mixtures; www.nrc.gov/reading-rm/doc-collections/gen-comm/info-notices/1986/in86043.html (URL); www.standort-ludwigshafen.basf.de/group/corporate/site-ludwigshafen/en/brand/IRGAGUARD (URL), Antibacterial application.

YU, Y., XIN, H.L., HOVDEN, R., WANG, D., RUS, E.D., MUNDY, J.A., MULLER, D.A., ABRUÑA, H.D. (2012) Three-dimensional tracking and visualization of hundreds of Pt−Co fuel cell nanocatalysts during electrochemical aging, Nano. Lett. 12, 4417-4423.

ZEWAIL, A. H., THOMAS, J. M. (2010) 4D Electron Microscopy. Imaging in Space and Time. Imperial College Press.

Tables

Parameters used for fast tomography analysis		values
Tilt	Start angle (°)	78
	End (°)	-38
	Amplitude (°)	116
	Total time (s)	226
Acquisition	Speed (°/s)	0.513
	Camera fps	≈7
	Video fps	≈20
Image	Image size (pixels)	1K x 1K
	Magnification	24,000
	Pixel resolution (nm/pixel)	0.8
Total number of frames of the uncompressed video (8 bit capture)		1584
Number of non-repeated frames		528
Number of exploitable (unblurred) frames		328

Table 1: Parameters of the fast tomography experiment performed in high vacuum at 20°C. The lower tilt limit (-38°) was due to some undesirable shadowing by the copper grid.

Temperature and environmental conditions		20°C, 6 10^{-7} mbar	280°C, 1.8 mbar O_2	450°C, 1.8 mbar O_2
Tilt	Start angle (°)	-25.5	-26.3	-25.7
	End (°)	42	35.7	42.2
	Amplitude (°)	67.5	62	67.9
Acquisition	Total time (s)	121	106	116
	Speed (°/s)	0.56	0.58	0.59
	Camera fps	≈7	≈7	≈7
	Video fps	≈20	≈20	≈20
Image	Image size (pixels)	1K x 1K	1K x 1K	1K x 1K
	Magnification	24,000	24,000	24,000
	Pixel resolution (nm/pixel)	0.8	0.8	0.8
Number of non-repeated frames		458	416	460
Number of exploitable (unblurred) frames		281	210	219

Table 2: Parameters of the OENT experiments performed between 20°C and 450°C.

Figures

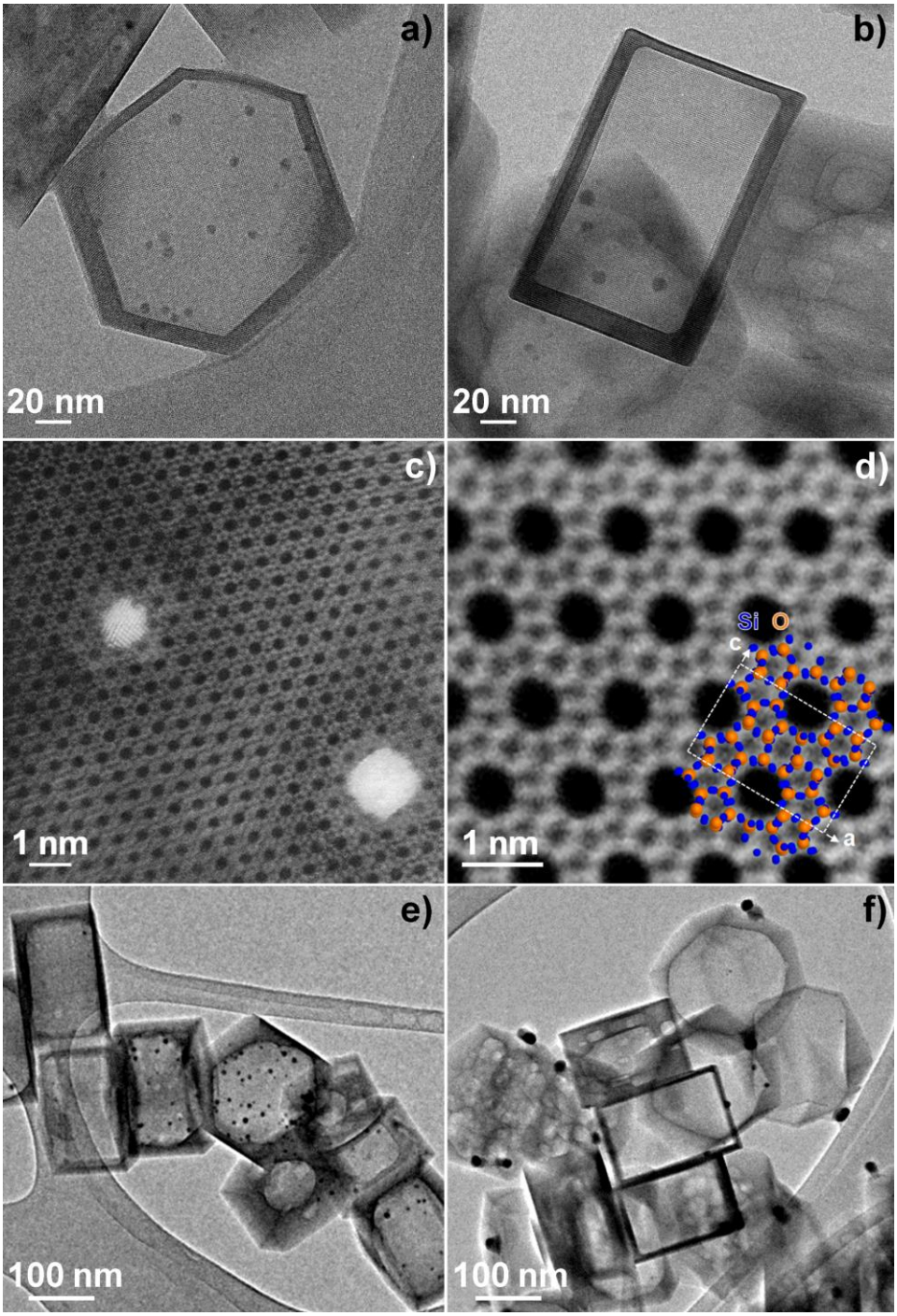

Figure 1: a-b) HTEM images of Ag nanoparticles in hollow silicalite-1 at 20°C under high vacuum (10^{-5} mbar) and at 430°C under 4 10^{-2} mbar O_2 respectively; it can be anticipated that both projections are along perpendicular axis. b-c) STEM imaging of the silicalite-1 atomic structure: two Ag nanoparticles are seen on the low mag image in c). The high magnification image (d) has been produced by averaging about 15 areas in order to increase the signal-to-noise ratio. As expected in STEM imaging, regions of high atomic densities appear in white (superimposed is the well-known model of silicalite MFI in the [010] projection http://www.iza-structure.org/databases/). d) TEM general view before the calcination; all Ag particles are inside the zeolite; e) sample after ex-situ calcination: Ag particles are bigger and outside the hollow silica.

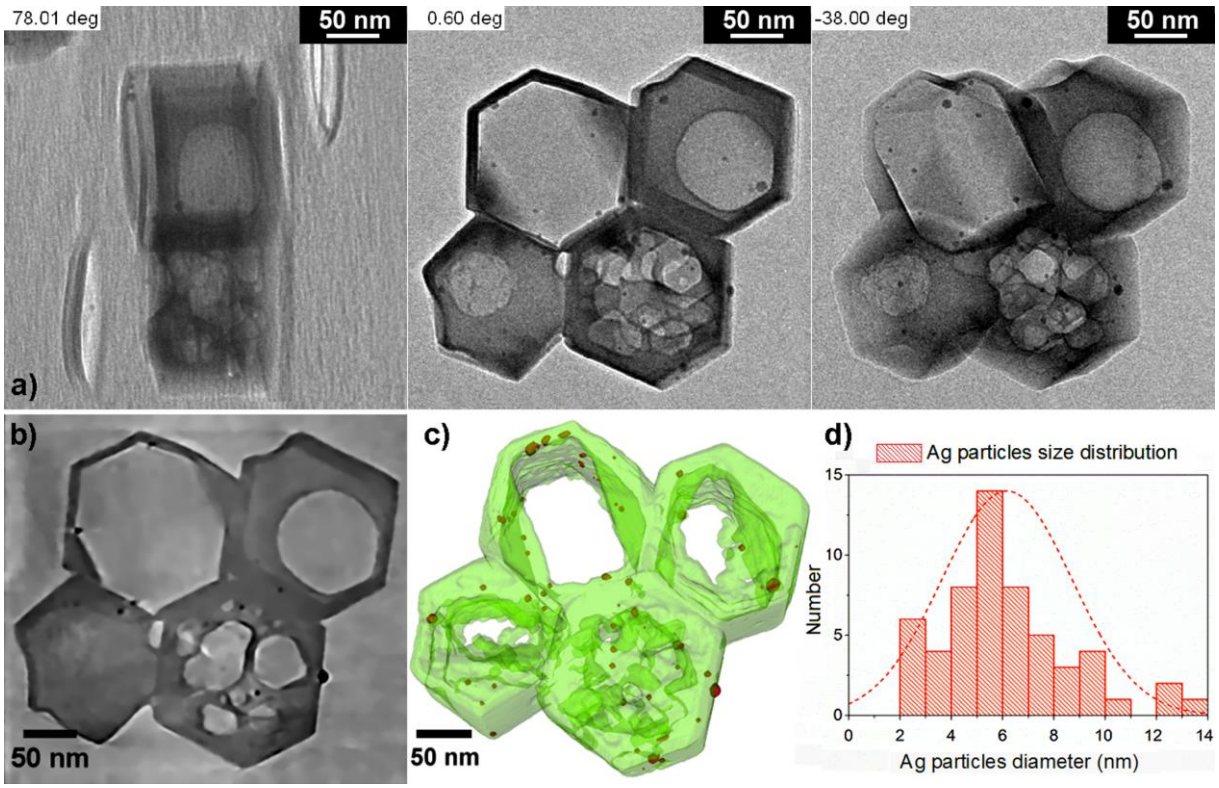

Figure 2: Fast tilting ET of hollow silicalite-1 zeolites with encaged Ag NPs performed in 226 seconds in high vacuum at 20°C. a): individual raw frames (after alignment and cropping) recorded at a tilt of 78, 0.6 and -38°, respectively. b) Cross section extracted from the reconstructed volume parallel to the XY plane roughly corresponding to the projection plane from the central image in a). The black dots represent the Ag NPs and dark grey corresponds to silica. c) Three dimensional model showing Ag nanoparticles in green and silica in red. d) Histogram representing the Ag NPs size distribution with an average of 6.1 nm and a standard deviation of 2.5 nm.

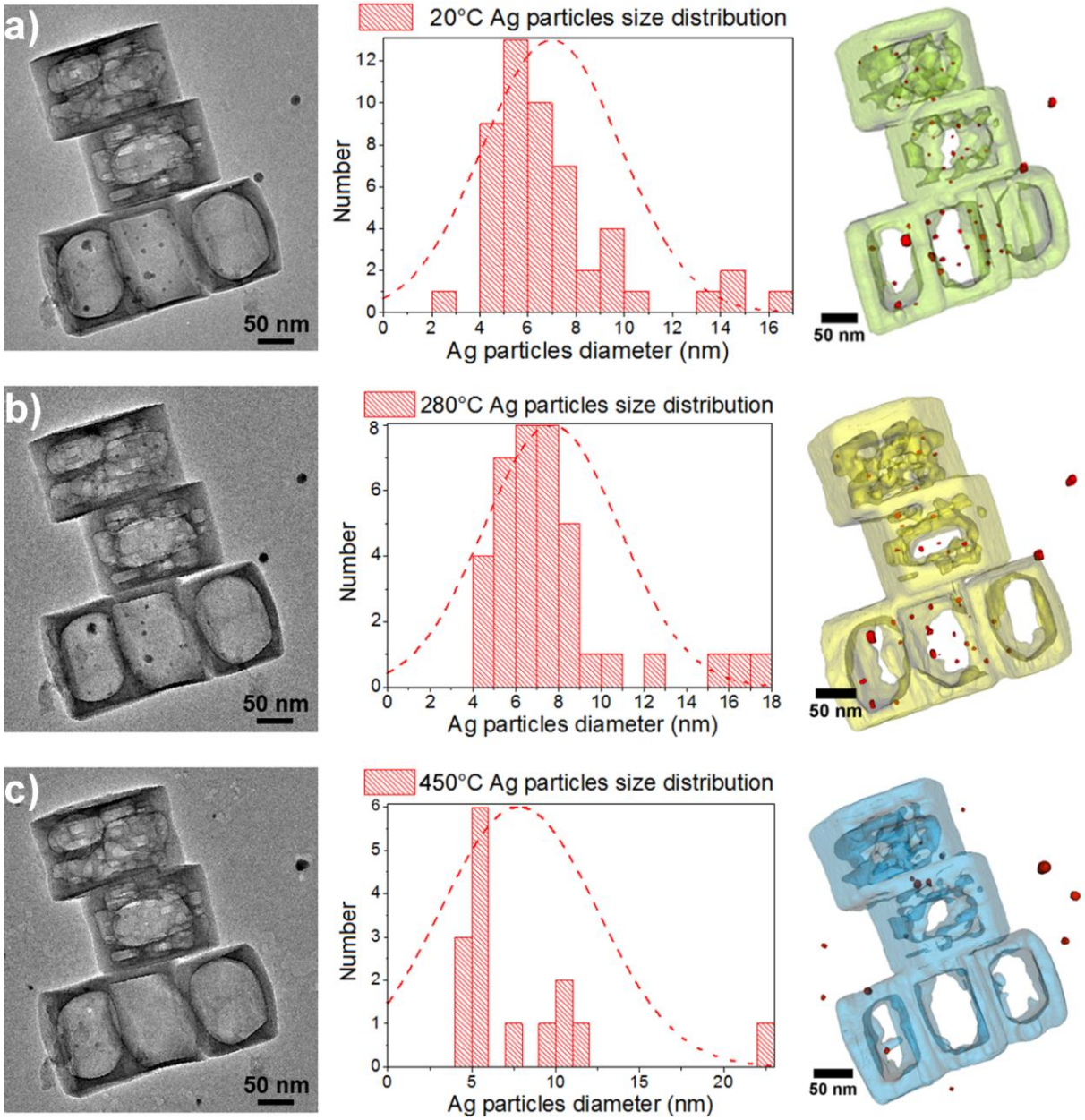

Figure 3: Calcination study by *operando* electron tomography of the same population of silicalite-1 hollow zeolites containing Ag NPs at a) 20°C in high vacuum, b) 280°C and c) 450°C under a 1.8 mbar of O_2. The left column shows experimental TEM images at 0° tilt (corresponding orthogonal XY sections from tomograms are shown in Figure SI2). In the centre are displayed the reconstructed models of the hollow silicalite-1 crystals with the zeolite in green, yellow and blue at 20, 280 and 450°C, respectively and Ag NPs in red. The right column displays the corresponding Ag particles size distributions. Average sizes are 6.9 nm, 7.6 nm and 7.8 nm at 20°C, 280°C and 450°C, respectively with standard deviations of 2.8 nm, 3.1 nm and 4.6 nm.

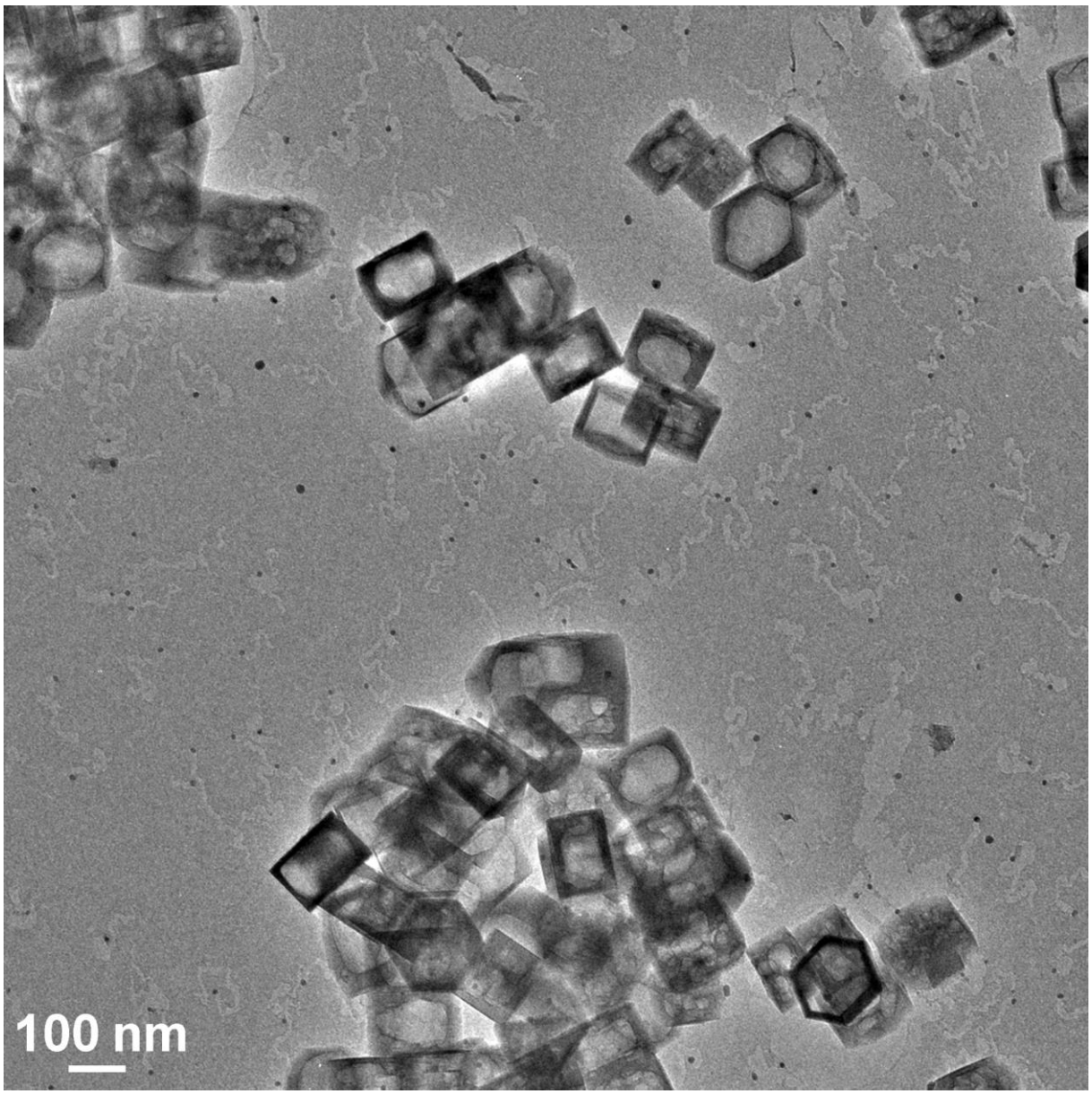

Figure 4: Carbon gasification due to O_2 dissociation at the surface of Ag nanoparticles (small dark dots) ejected outside the silicalites as observed at 450°C under an oxygen partial pressure 0.1 mbar.

SUPPLEMENTARY INFORMATION

SI-1. IRRADIATION TESTS

The video (SI_OENT_L-Roiban_et-al_speedX200.avi) illustrates the irradiation behaviour of a group of silica hollow zeolites submitted to a 4 minutes exposure at different electron fluxes respectively: $1.1 \cdot 10^7$ $e^- nm^{-2} s^{-1}$, $4.4 \cdot 10^6$ $e^- nm^{-2} s^{-1}$ and $3.3 \cdot 10^6$ $e^- nm^{-2} s^{-1}$ (from left to right; the 3 sequences were accelerated 200 times in order to allow an easier perception of the morphological changes - meaning damages - during the observation) . Contrarily to the two first conditions, the last condition does not reveal any significant morphological evolution of the hollow silicates during the exposure to the electron beam; the corresponding electron flux and exposure time were then chosen as maximal limits to perform safe electron tomography analysis.

SI-2. CONTIUNOUS ROTATION FAST TOMOGRAPHY

Among the 528 non-repeated images acquired during the continuous rotation sequence related to figure 2, 200 frames were eliminated according to their poor sharpness (see Figure SI1a-d)). The analysis of the reconstructed volume allowed to access of an important set of morphological information concerning the hollow silica zeolites and the particles size distribution. It was observed that the hollow silica zeolites have a hexagonal basis and that walls have a thickness varying from 4 nm to 34 nm (Figure SI1e-g)). Other features are discussed in the main text.

SI-3. OPERANDO ELECTRON TOMOGRAPHY

The important height of the Gatan heating holder produces rapidly a severe shadowing of the object when the sample is tilted; as a consequence, the usable tilting amplitude is limited to about 72° with this holder. In the present case the tilt series in operando mode at 20°C (in high vacuum), 280°C and 450°C under 1.8 mbar of O_2, were acquired within a short angular interval around -26° to +42° as reported in Table 2 from the main text. This unfortunately leads to a large missing wedge in the acquired data. According to a very similar goniometer rotation speed as shown in Table 1, the acquisition time of each tilt series with such a reduced tilt amplitude dropped down to less than two minutes.

Figure SI2 illustrates the reconstructed tomograms from the 3 series. An a priori knowledge of the polyhedral shape of the cages was deduced from the fast tomography described by Figure 2. This information, especially the existence of a hexagonal basis of the hollow zeolites, has greatly facilitated the data segmentation of these operando experiments, owing to the large missing wedge. This missing information also led to a poor resolution along Z, since slices extracted at the middle of tomograms did not properly evidence the thinnest parts of the silica walls expected around 4 nm (Figure SI2). Nevertheless, with the help of the a priori morphological knowledge the modeling and the quantification of the operando electron tomography volumes was possible.

SI-4: CARBON GASIFICATION BY SILVER NPS UNDER O_2 PRESSURE

When the organic residues blocking the pores of the zeolites have been consumed under oxygen, volatilized silver diffuses out of the cages and metallic nanoparticles reform on the carbon film.

Carbon gasification induced by the dissociation of O_2 molecules at their surfaces leads to a progressive consumption of the carbon supporting film and most of the silver nanoparticles create trenches as shown in Figure 4 (main text). The carbon gasification process can be followed in situ under environmental conditions, i.e. oxygen partial pressure and in temperature (according to our experimental conditions, between about 0.1 - 2 mbar and 450 - 500°C).

Figure SI3 reports High Resolution micrographs of two nanoparticles advancing during this process; the lattice contrast visible on all images indicate that silver remains crystalline. The oxygen pressure has been slightly reduced here as compared to the OENT experiments - Figure 3 - to slow down the process. Note the wavy form on the front surfaces in contact with the carbon film where oxygen molecules are permanently dissociated into oxygen atoms reacting with amorphous carbon to produce CO_2 gas.

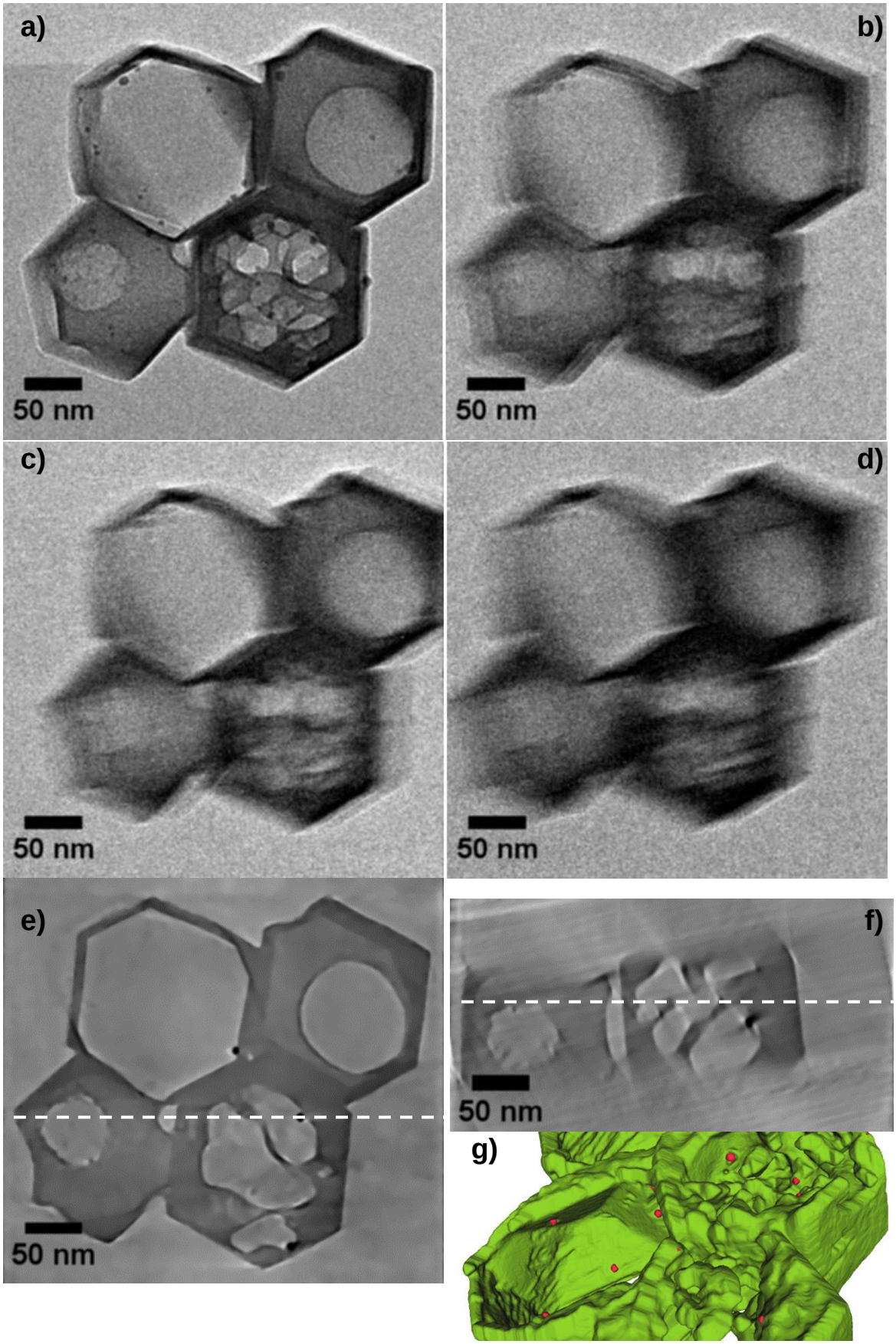

Figure SI1: a-d) Examples of blurred images automatically extracted from the continuous tilt series; the first image a) of the series is an unblurred image serving as a reference to define a blur

criterion on the basis of the contrast sharpness. e-f) Orthogonal XY and XZ cross sections extracted from the reconstructed volume; dashed lines are the intersections of the two slices. g) detail of the 3D model of the hollow silica zeolite showing the internal morphology of the walls (in green) and the positions of Ag particles (in red).

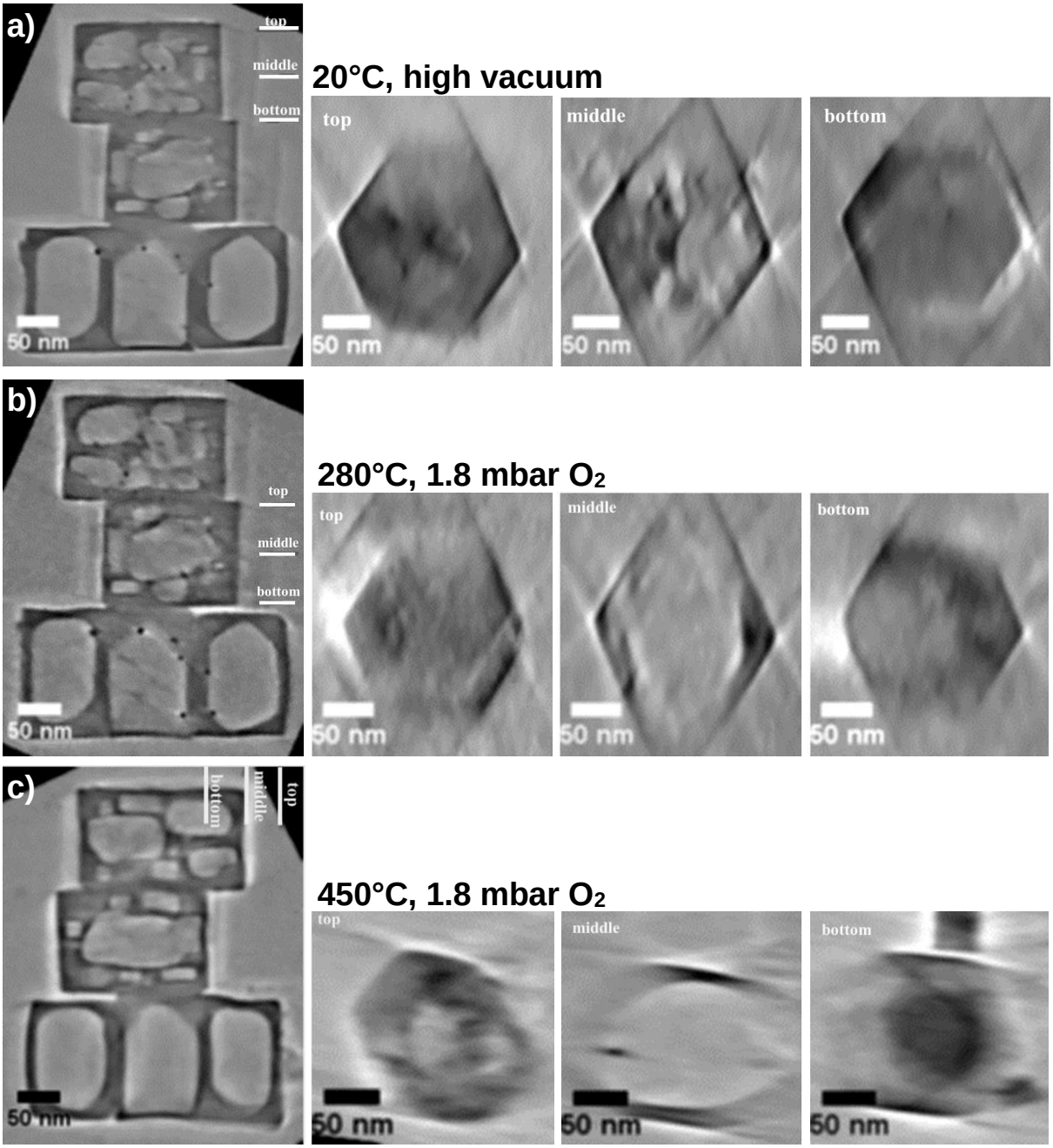

Figure SI2: Operando electron tomography: oriented cross sections extracted from the reconstructed volumes at 20°C (high vacuum), 280°C and 450°C under 1.8 mbar of O_2 (respectively from a) to c)). X-Y Slides of the tomograms are shown on the left; the position of intersection of the orthogonal slices extracted on the top, middle and bottom of one of the hollow silica zeolites are indicated in all volumes. At 20°C and at 280°C the Ag nanoparticles are visible inside the cages contrarily to the case at 450°C. On the top and bottom cross sections of the hollow silica zeolites the hexagonal shape of basis can be distinguish. In the middle cross sections the resolution did not allow to resolve any more the 4 nm silica wall thickness in the Z direction.

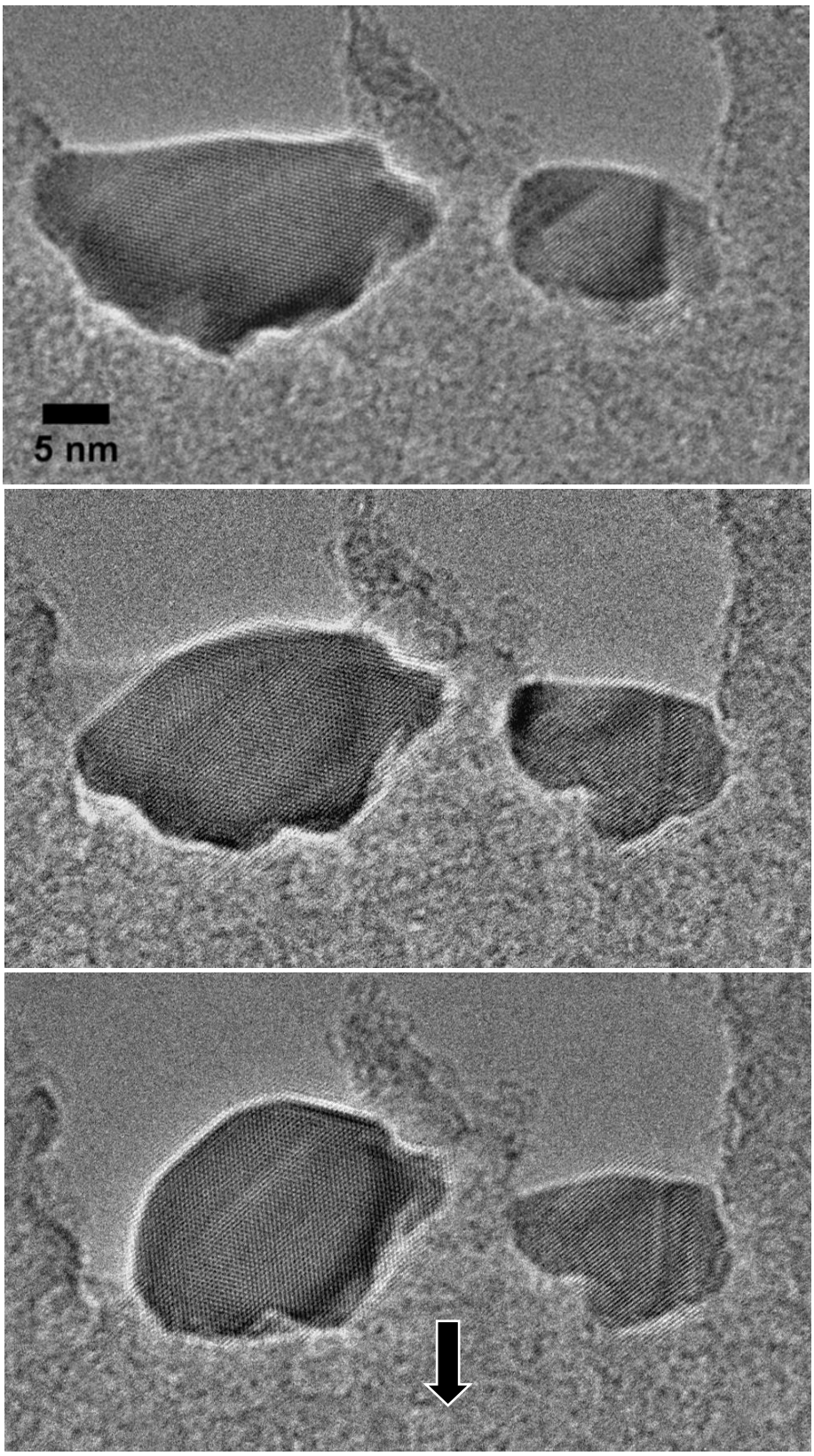

Figure SI3: The 'Pacman' sequence as followed at atomic resolution under 0.6 mbar at 495°C. From top to bottom: successive images at 1.6 sec intervals showing the advances of two Ag nanoparticles onto the carbon supporting film. The arrow indicates the mean direction of motion of both nanoparticles; the one on the left is permanently in the [110] orientation.